NUMERICAL SIMULATION OF COMBUSTION IN KEROSENE FUELED RAMP CAVITY BASED SCRAMJET COMBUSTOR

Ramesh Behera* and Debasis Chakraborty*

Abstract

The flow field of a ramp cavity based scramjet combustor with kerosene fuel is explored numerically using commercial CFD software. Three-dimensional Navier-Stokes equations are solved alongwith $K - \varepsilon$ turbulence model and fast rate chemical kinetics. Liquid kerosene is considered as disperse phase fluid and is modeled through Lagrangian tracking method. Simulation captures all essential features of the flow field. Good agreement between computational and experimental values forms the basis of further analysis. The flow phenomena in the combustor are presented through the distribution of important thermochemical parameters at different cross sections. Normal shock is seen to occur in the combustor and significant upstream interaction was observed due to heat release. The computed combustion efficiency is near unity as the fuel equivalence ratio is small.

Introduction

The success of an efficient design of hypersonic air-breathing cruise vehicle largely depends on proper choice of propulsion system. This type of vehicle, according to current proposal, will use Scramjet propulsion system. Both hydrogen and hydrocarbon fuels are considered depending on the application and speed range. Although, hydrogen is having a lot of attractive features in terms of specific impulses, ignition characteristics etc., energy density and handling issues render liquid hydrocarbon as very good candidate in lower hypersonic flight regimes in a volume limited applications. In a recent comprehensive review on Scramjet technologies, Curran [1] has identified two emerging Scramjet applications namely (1) hydrogen fueled engine to access space and (2) hydrocarbon-fueled engines for air-launched missiles.

All the issues related to the hypersonic inlet, isolators, liquid fuels, wall fuel injection, axial fuel injection, combustor, and nozzle of the liquid fuel Scramjet have been reviewed extensively by Waltrup [2]. Considerable efforts have been focused on different injection schemes for different geometrical configurations and flow conditions in the past two decades. Selected methods that have been used to enhance the mixing process in the Scramjet engines are summarized and reported in Ref 3. Issues related to liquid hydrocarbon fuel injection in supersonic cross-flow and effective flameholding mechanisms continued to be active research topics [4-8]. The cavity based integrated configuration, including fuel injector and flameholder, has been shown to possess a great potential to achieve active flame stabilization in supersonic combustor. Liquid fuel can be injected at the floor of the cavity or upstream. With a cavity, a high temperature, low speed recirculation zone can be established to serve as a pilot flame, which in turn can reduce the bulk ignition delay time and sustain a stable combustion. Experiments [7, 9-10] have shown that the use of a cavity after the ramp-injector significantly improves the hydrocarbon combustion efficiency in a supersonic flow. The schematic of the flow field in the ramp-cavity combustor is shown in Fig. 1.

The ramp injectors are very helpful to produce both axial and contra rotating vortices. The axial vortices possesses a better far field characteristic while the contra rotating vortices created at the base of the ramp can help in flame stabilization. The increase in pressure and temperature due to compression due to ramp surface create favorable condition for ignition. Furthermore, wall injection can greatly simplify the design of the combustor and cooling system as compared to the in-stream devices.

The physical mechanism of the effects of cavity-based flameholder on supersonic combustion is quiet complex and not properly understood. The existing definition of characteristics of open and closed cavities is based on

* Computational Combustion Dynamics Division, Directorate of Computational Dynamics, Defence Research and Development Laboratory, Kanchanbagh Post, Hyderabad - 500 058, India; Email: debasis_ccd@drdl.ernet.in
Manuscript received on 06 Jul 2005, Paper reviewed, revised and accepted on 03 Feb 2006

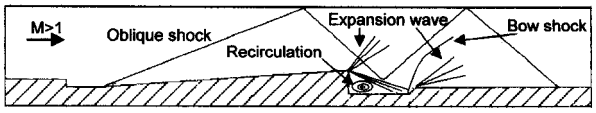

Fig.1 Schematic of flow field in ramp-cavity combustor

nonreacting flows and subject to revision for the reacting flow situation. Efforts are continuing [11] to understand the stable and unstable characteristics of the cavity flow with an emphasis on the phenomena of flow-induced cavity resonance. It is generally recognized that open cavities (L/D <10) could be used for flameholding while the mixing enhancement can be achieved through the close cavities (L/D>10).

With the advent of powerful computer, robust numerical algorithm, Computational Fluid Dynamics (CFD) techniques are routinely used for the design and analysis of scramjet propulsion system. To accurately model scramjet flow field, CFD must adequately resolve several complex physical processes including: three-dimensional shock-boundary layer interaction, turbulent mixing of high speed subsonic and supersonic streams and kinetics of hydrocarbon fuels. Although, a large volume of literature exists on numerical simulation of hydrogen combustion in scramjet combustor, the simulation of hydrocarbon combustion in scramjet is comparatively small, mostly, because of complexity of modeling hydrocarbon fuel. Majority of the work on hydrocarbon combustion in scramjet propulsion system is limited to relatively simple ethylene fuel. Carson et. al [12] have numerically studied ethylene combustion in a backward facing stepped scramjet combustor using a single step chemical kinetic. Their parametric studies with two different step heights (3.2 mm and 6.4 mm) reveals that the lower step height does not necessarily ensure better efficiency. Abdel-Salam et. al [13] have used Fluent Software to study the flow field of scramjet combustor with both hydrogen and ethylene fuel. Baurle and Eklund [14] have studied cavity based scramjet combustor with ethylene fuel using VULCAN [15] Navier Stokes Solver. Turbulence is modeled with Menter's SST [16] model while a 3 step 6 species reduced model is employed to describe the chemical kinetics. Two-flight conditions corresponding to flight Mach No. 4 and 6.5 are simulated to address the problem of dual mode ramjet- scramjet operation. The computed results are shown to be very sensitive to the modeled level of heat and mass transfer. Dufour and Bouchez [17] have numerically simulated the scramjet experiment [18] with kerosene fuel using a three dimensional Navier Stokes solver and single step chemical kinetics. A reasonable good match is obtained between the computed and experimentally measured wall static pressure. It proceeds from the results that the pressure recovery and combustion efficiency can be predicted confidently from the simulation. These computations confirmed that, for the specific injector design investigated, the combustion efficiency is limited by an imperfect mixing between fuel and air.

In this work, three dimensional viscous simulations have been carried out for the experimental condition of ramp-cavity based kerosene fueled model scramjet combustor test [19] in connect pipe mode facility using a commercial CFD Software. The computed and measured values of surface pressure are compared. Analysis of the complex flow field of kerosene fueled scramjet combustor is presented from the numerical simulation.

Methodology

The software, used in the present study, is a three dimensional Navier Stokes code - CFX-TASCFlow [20] which is an integrated software system capable of solving diverse and complex multidimensional fluid flow problems. The code is fully implicit, finite volume method with finite element based discretisation of geometry. The method retains much of the geometric flexibility of finite element methods as well as the important conservation properties of the finite volume method. It utilizes numerical upwind schemes to ensure global convergence of mass, momentum, energy and species. It implements a general non-orthogonal, structured, boundary fitted grids. In the present study, to circumvent the initial numerical transient, the descretisation of the convective terms are done by first order upwind difference scheme till few time steps and subsequently, the convective terms are discretized through 2nd order scheme to capture the flow features more accurately. The turbulence model used was $K-\varepsilon$ model with wall functions

Governing Equations

The appropriate system of equations governing the turbulent flow of a compressible gas may be written as:

Continuity equation:

$$\frac{\partial \rho}{\partial t} + \frac{\partial}{\partial x_k}(\rho\, u_k) = 0 \qquad k = 1,2,3$$

Momentum equation: ,

$$\frac{\partial}{\partial t}(\rho\, u_i) + \frac{\partial}{\partial x_k}(\rho\, u_i\, u_k) + \frac{\partial P}{\partial x_i} = \frac{\partial\, (\tau_{ik})}{\partial x_k}, \qquad i, k = 1,2,3$$

Energy equation:

$$\frac{\partial}{\partial t}(\rho H) + \frac{\partial}{\partial x_k}(\rho u_k H) = -\frac{\partial}{\partial x_k}(u_j \tau_{jk}) + \frac{\partial q_k}{\partial x_k}, \quad j, k + 1,2,3$$

Turbulent kinetic energy (K) equation:

$$\frac{\partial}{\partial t}(\rho K) + \frac{\partial}{\partial x_k}(\rho u_k K) = \frac{\partial}{\partial x_k}\left(\left(\frac{\mu_l}{Pr} + \frac{\mu_t}{\sigma_K}\right)\frac{\partial K}{\partial x_k}\right) + S_K$$

Rate of dissipation of turbulent kinetic energy (ε) equation:

$$\frac{\partial}{\partial t}(\rho \varepsilon) + \frac{\partial}{\partial x_k}(\rho u_k \varepsilon) = \frac{\partial}{\partial x_k}\left(\left(\frac{\mu_l}{Pr} + \frac{\mu_t}{\sigma_\varepsilon}\right)\frac{\partial \varepsilon}{\partial x_k}\right) + S_\varepsilon$$

Species mass fraction (Z):

$$\frac{\partial}{\partial t}(\rho Z) + \frac{\partial}{\partial x_k}(\rho u_k Z) = \frac{\partial}{\partial x_k}\left(\left(\frac{\mu_l}{Pr} + \frac{\mu_t}{\sigma_c}\right)\frac{\partial Z}{\partial x_k}\right)$$

where, ρ, u_i, p, H are the density, velocity components, pressure and total energy respectively and $\mu = \mu_l + \mu_t$ is the total viscosity; μ_l, μ_t being the laminar and turbulent viscosity and Pr is the Prandtl number. The source terms S_k and S_ε of the K and ε equation are defined as

$$S_K = \tau_{ik}\frac{\partial u_i}{\partial x_k} - \rho\varepsilon \text{ and } S_\varepsilon = C_{\varepsilon 1}\tau_{ik}\frac{\partial u_i}{\partial x_k} - C_{\varepsilon 2}\frac{\rho\varepsilon^2}{K}$$

where turbulent shear stress is defined as

$$\tau_{ik} = \mu_t\left(\frac{\partial u_i}{\partial x_k} + \frac{\partial u_k}{\partial x_i}\right)$$

Laminar viscosity (μ_l) is calculated from Sutherland law as

$$\mu_l = \mu_{ref}\left(\frac{T}{T_{ref}}\right)^{3/2}\left(\frac{T_{ref} + S}{T + S}\right)$$

where, T is the temperature and μ_{ref}, T_{ref}, and S are known values. The turbulent viscosity μ_t is calculated as

$$\mu_t = c_\mu \frac{\rho K^2}{\varepsilon}$$

The coefficients involved in the calculation of μ_t are taken as

$c_\mu = 0.09$, $C_{\varepsilon l} = 1.44$, $C_{\varepsilon 2} = 1.92$

$\sigma_K = 1.0$, $\sigma_\varepsilon = 1.3$, $\sigma_c = 0.9$

The heat flux q_k is calculated as $q_k = -\lambda\frac{\partial T}{\partial x_k}$, λ is the coefficient of thermal conductivity

Combustion Modelling

For combustion, the eddy dissipation combustion model is used for its simplicity and robust performance in predicting reactive flows. The eddy dissipation model is based on the concept that chemical reaction is fast relative to the transport process in the flow. When reactants mix at the molecular level, they instantaneously from products. The model assumes that the reaction rate may be related directly to the time required to mix reactants at molecular level. In turbulent flows, this mixing time is dictated by the eddy properties and therefore the burning rate is proportional to the rate at which turbulent kinetic energy is dissipated i.e., reaction rate is proportional to ε/K, where K is the turbulent kinetic energy and ε is its rate of dissipation. The chemistry of the combustion reaction is represented on a molar basis by: $C_{12}H_{23} + 17.75O_2 = 12CO_2 + 11.5H_2O$. The mixing rate determined from the Eddy Dissipation Model (EDM) is given as.

$$R_{k,edm} = -A_{ebu}\rho\frac{\varepsilon}{K}\min\left\{Y_f, \frac{Y_o}{r_k}, B_{ebu}\frac{Y_p}{1 + r_k}\right\}$$

where ρ, Y_f, Y_o and Y_p are the density and mass fractions of fuel, oxidizer and products respectively, A_{ebu} and B_{ebu} are the model constants and r_k is the stoichiometric ratio.

Discrete Phase Model

Lagrangian tracking method is used for discrete phase model to characterize the flow behaviour of the dispersed phase fluid (kerosene liquid). The prediction of flows involving the dispersed phase involves the separate calculation of each phase with source terms generated to account for the interaction between the phases. The flow of the continuous phase is predicted using a discretized form of the Navier Stokes equations. With the dispersed phase there is no continuum, and each particle interacts with the fluid and other particles discretely. Therefore, the most

widely applied method available to determine the behaviour of the dispersed phase is to track several individual particles through the flow field. Each particle represents a sample of particles that follow an identical path. The behaviour of the tracked particles is used to describe the average behaviour of the dispersed phase. Only viscous drag on the particles is considered in the study. Particle/particle interactions and effect of turbulence in the discrete phase are not simulated in the analysis.

Source Terms for Governing Equations

For the purpose of describing the types of sources generated by particles, it is convenient to consider the differences between inert and reacting particles. Both inert and reacting components of particles exchange momentum with the fluid due to viscous drag and exchange energy due to particle heating. Reacting particles may also exchange mass with the fluid as well as exchange momentum and energy due to mass sources. If the sources are grouped according to inert components (those sources common to all particle types) and reacting components (those sources only found with reacting particles) then particle sources may be generalized as shown in Table 1. The details of the formulation is available in Ref. 20.

Source	Inert component	Reacting component
mass	-----	$\dot{N}\delta m_p$
momentum	$\dot{N} m_p (v_p - v_f)\left[1-\exp\left(\frac{-18\mu\delta t}{\rho d^2}\right)\right]$	$\dot{N}\delta m_p v_p$
energy	$\dot{N}\int_0^{\delta t} h_c A_p (T_f - T_p)dt$	$\dot{N}(-L_v\delta m_v + Q_c\delta m_c)$

δt = time step over which sources are applied

$\dot{N}$ = number of particles injected per unit time along the path

δm_p = mass loss of a particle in time step, δt

h_c = convective heat transfer coefficient per unit area, A_p

$L_v\,\delta m_v$ = energy required to vaporize volatiles of mass, δm_v

$Q_c\delta m_c$ = energy generated in burning char of mass, δm_c

T_p, T_f = particle and fluid temperature

ρ, μ, d = density, viscosity, and diameter of particle respectively

v_f, v_p = fluid and particle velocity

Discretisation of Governing Equations

The CFX-TASCFlow solver utilizes a finite volume approach, in which the conservation equations in differential form are integrated over a control volume described around a node, to obtain an integral equation. The pressure integral terms in the momentum integral equation and the spatial derivative terms in the integral equations are evaluated using finite element approach. An element is described with eight neighboring nodes. The advective term is evaluated using upwind differencing with physical advection correction. The set of discretised equations form a set of algebraic equations: $A\vec{x} = b$ where $\vec{x}$ is the solution vector. The solver uses an iterative procedure to update an approximated x_n(solution of x at n^{th} time level) by solving for an approximate correction x' from the equation $A\vec{x'} = \vec{R}$, where $\vec{R} = \vec{b} - A\vec{x_n}$ is the residual at n^{th} time level. The equation $A\vec{x'} = \vec{R}$ is solved approximately using an approach called Incomplete Lower Upper factorization method. An algebraic multigrid method is implemented to reduce low frequency errors in the solution of the algebraic equations. Maximum residual $(= \phi_j^{n+1} - f(\phi_j^{n+1}, \phi_j^n)) < 10^{-4}$ 10^{-4} is taken as convergence criteria

Results and Discussions

The combustor configurations for which the present computations are carried out are taken from Ref. 19. The combustor configuration is presented in Fig. 2 (a). The combustor consists of three parts namely, the facility nozzle of length 5.7 d (d is the throat height of the facility nozzle) to get a Mach 2 at combustor entry, the constant area section of length of 30.6 d where the ramps, cavities and fuel injectors are provided and the divergent section of length of 25 d of divergence 3.2°. Three and two distributed ramps of length 12.5 d are provided at a distance of 5d from the combustor entry on the bottom and top walls respectively in the constant area portion of the combustor as shown in Figs. 2(b) and 2 (c). The ramp

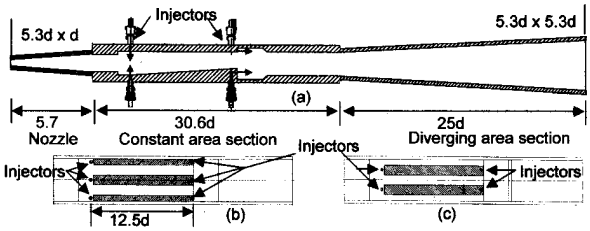

Fig. 2 Ramp cavity scramjet combustor configuration: (a) Full combustor, (b) Bottom plate of constant area section, and (c) Top plate of constant area section

injectors are considered to generate both axial and contra rotating vortices for better mixing and subsequent reactions. The precompression by the ramp face and the stagnation region near the leading edge of the ramp injectors are supposed to create favorable conditions for ignition. One cavity each of length to depth ratio of 7.25 is placed in both top and bottom wall at the end of the ramps for flame holding purpose. Kerosene is injected in the combustor through 10 numbers of injectors of 0.4mm diameter. Five numbers of transverse injectors (03 from top wall and 02 from bottom wall) are placed at 4.7 d from the combustor entry and another five numbers of parallel injectors (02 from top wall and 03 bottom wall) are provided from the base of the ramps to the cavities (fuel injector locations are indicated in Fig. 1). Although barbotaging of kerosene fuel with hydrogen have been employed in the experimental investigation, the simulation does not consider this aspect. The computational domain starts from the throat of the two-dimensional facility nozzle in order to take a realistic boundary layer profile at the combustor entry and also to capture any upstream interaction that may arise due to heat release in the combustor. The vitiated air from the burner is accelerated through a two dimensional convergent-divergent nozzle of Mach 2.0 into the combustion chamber. The total temperature and total pressure of the vitiated air is 0.9 MPa and 1645 K respectively. Composition of the vitiated air i.e., the mass fraction of N_2, H_2O and O_2 is 0.5697, 0.2287 and 0.2016 respectively. The mass flow rate of vitiated air is 0.9617 Kg/sec whereas kerosene is injected at 16.8 gm / sec at an equivalence ratio of 0.21.

The schematic of the computational domain is presented in Fig. 2. The domain starts from the throat of the facility nozzle. Taking the advantage of geometrical similarity, only one half of the combustor is considered as the computational domain. A total number of 182 x 61x 23 numbers of structured grids are used in the simulation. The typical grid distribution X-Y, X-Z and Y-Z planes are shown in Figs. 3(a), 3(b) and 3(c) respectively. The grids are fine near the injection holes, wall region, ramp and cavity zone, while relative coarser grids are provided in the remaining portion of the combustor. In the simulation, X-axis is taken along the length of the combustor while; Y and Z axes are along the height and width of the combustor respectively. The origin is placed at throat center of the facility nozzle. Since the injection holes are very small in diameter, original grids are made fine by doing the grid embedment adjacent to each injection point. Grid embedding has been made 3 to 5 time in X, Y and Z direction as per requirement. As the computational domain starts from the throat of the facility nozzle, sonic conditions are applied at the inflow plane. No slip and adiabatic wall boundary conditions are imposed at the wall. As the experiment was performed in the atmospheric condition, atmospheric pressure has been imposed in the out flow boundary. Symmetry condition is applied at the plane of symmetry. Log normalized maximum residue 10^{-4} is considered as the convergent criteria.

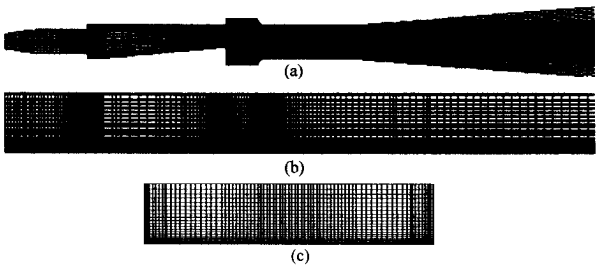

Fig. 3 Grid structure of the computational domain (182 x 61 x 23): (a) X-Y plane, (b) X-Z plane, and (c) Y-Z plane.

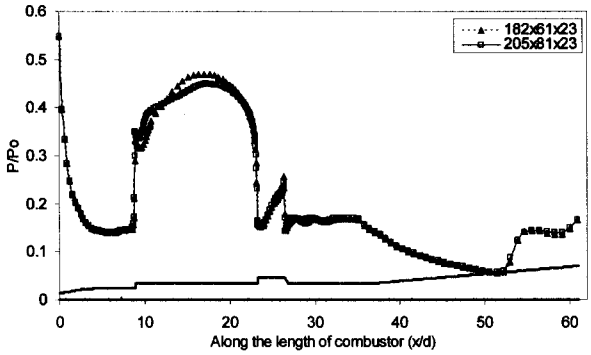

Fig. 4 Comparison of pressure distribution at the top surface of the symmetry plane for two different grids

The grid independence study is performed with total pressure and total temperature of 0.6 MPa and 1490 K, respectively with other conditions as mentioned above. The axial distribution of surface pressure at the top surface in the symmetry plane is compared in Fig. 4 for two different grids namely 182 x 61 x 23 and 205 x 81 x 23. Values of surface pressure change a little with the change of grid, thus proving the grid independence of the results.

The qualitative features of the flow field in the combustor are presented through the description of the important thermo-chemical parameters in the symmetry plane and in various cross sectional planes in the combustor. Mach number distribution for the reacting and non-reacting cases in the plane of symmetry is compared in Fig. 5. The flow structure is different between the two cases.

The terminal shock for the reacting case is positioned in the upstream location (compared to the nonreacting case) because of heat release due to reaction. The flow accelerates again in the divergent section of the combustor. The comparison of temperature distribution between the reacting and non-reacting case in the plane of symmetry is shown in Fig. 6. The high temperature region at the ramps and the cavities indicate the zone of reaction. The cross sectional view of the Mach number and temperature in the reacting case at various axial stations x/d = 8, 17, 23, 27, 36, 49 (d is the height of the throat) are shown in Fig. 7. The axial stations are so chosen that flow properties can be seen at important locations of the combustor. The cross sectional view of the oxidizer mass fraction (Y_{O2}) and the product mass fraction (Y_{CO2}) is shown in Fig. 8. Significant amount of oxygen is seen to remain unused even at x/d =49. Liquid kerosene trajectory from the injection point is presented in Fig. 9. The liquid droplets are seen to vaporize in the combustor. The axial distribution of the computed non-dimensional surface pressure (P/P_0), (P_0 being the stagnation pressure) at the top surface of the plane of symmetry is compared with the experimental values in Fig. 10. The axial length has been normalized with the height of the throat of the facility nozzle. A very good match has been obtained within experiment and numerical value except near the injection location, where the computation predicts higher value. High heat release associated with the fast chemistry assumption in combustion modeling is the cause for higher pressure in the prediction. The comparison of axial distribution of mass averaged Mach number between reacting and non-reacting case are shown in Fig. 11. Mach number is seen to be less than one between x/d=6 to 23 for reacting case. The flow is seen to accelerate in the downstream locations. The combustion efficiency and the normalized total pressure for the reacting case are shown in Fig. 12. Combustion efficiency (η) is defined as the ratio of the actual CO_2 formed to the ideal CO_2, which can be formed from the reaction. Normalized total pressure (Π) is defined as:

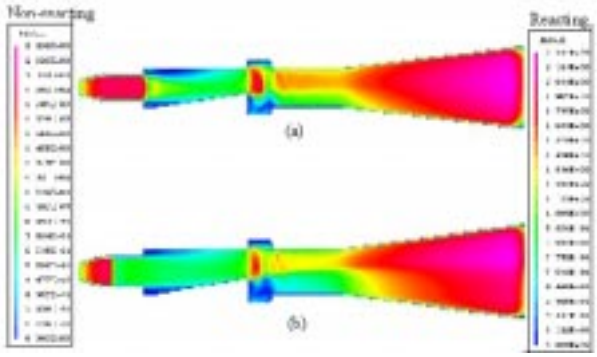

Fig. 5 Mach number distribution in symmetry plane: (a) non-reacting and (b) reacting

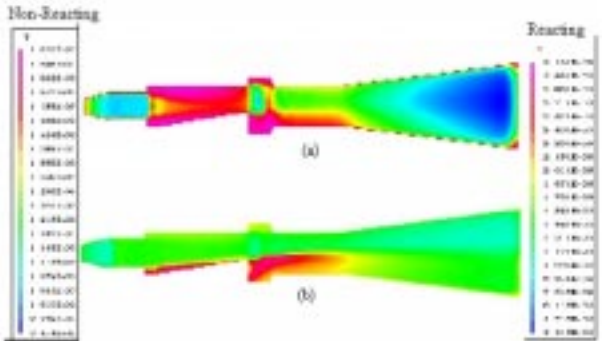

Fig. 6 Temperature distribution in symmetry plane: (a) non-reacting and (b) reacting

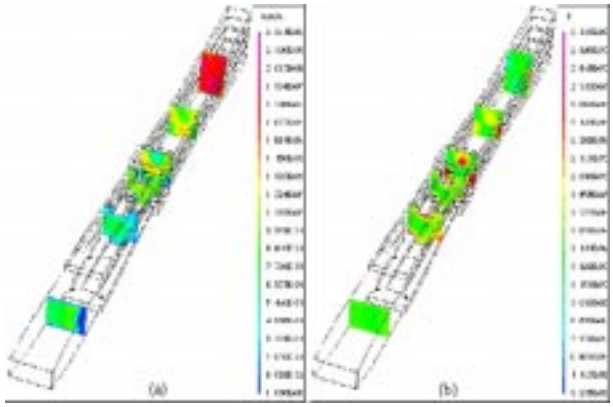

Fig. 7 (a) Mach number, and (b) Temperature distribution at different axial locations at x/d = 8, 17, 23, 27, 36, 49

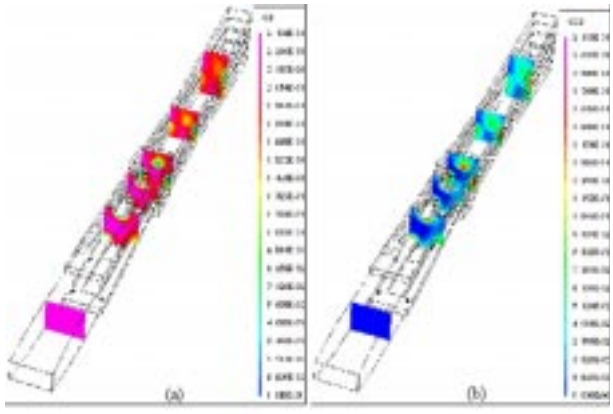

Fig. 8 (a) Y_{O2}, and (b) Y_{CO2} distribution at different axial locations at x/d = 8, 17, 23, 27, 36, 49

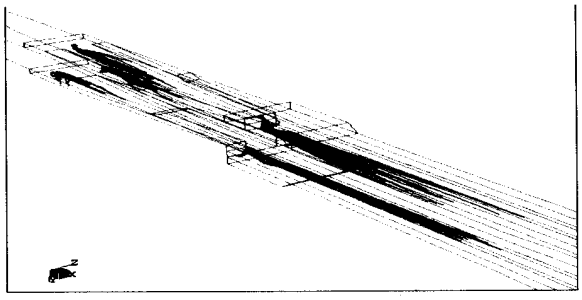

Fig. 9 Liquid kerosene trajectory in the combustor

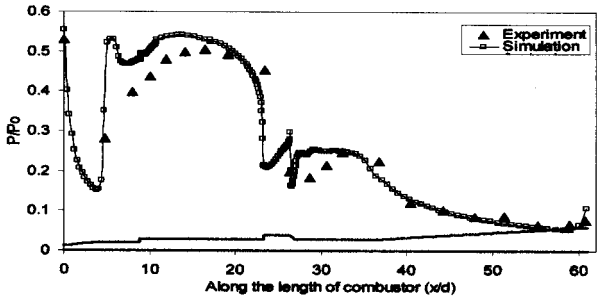

Fig. 10 Comparison of axial top surface pressure distribution at symmetry plane between experiment and computation for reacting case

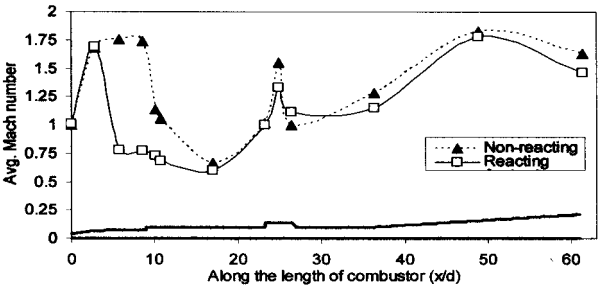

Fig. 11 Comparison of axial variation of mass averaged Mach number for the non-reacting and reacting cases

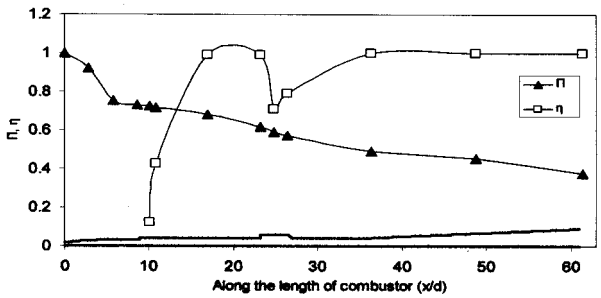

Fig. 12 Axial variation of normalized total pressure and Combustion efficiency

$$\Pi = \frac{\dfrac{\int_A \rho u P_0 dA}{\int_A \rho u dA}}{\left(\dfrac{\int_A \rho u P_0 dA}{\int_A \rho u dA}\right)_{inlet}}$$

From the axial distribution of the combustion efficiency (η), it is clear that the fuel injected with equivalence ratio 0.105 from the transverse injectors at (x/d = 10) is consumed within x/d = 17 and the rest of the fuel from the parallel injector at (x/d = 23) is oxidized within x/d = 36. Total pressure ratio is seen to decrease with the axial distance signifying the losses through shocks, mixing and combustion.

Conclusions

Numerical simulations are presented in a model ramp cavity combustor using a commercial CFD Software, CFX-TASCflow. Three dimensional Navier Stokes equations are solved along with K - ε turbulence model and fast rate chemical kinetics. The computations are carried out from throat of the facility nozzle to capture the upstream interaction. The simulations capture all the essential features of the flow field. The computed surface pressure matches well with the experimental value. The normal shock is seen to occur at x/d =4 due to high blockage in the combustor. For reacting case, the heat release due to reaction pushed the terminal shock in the upstream positions. The combustion efficiency is near unity as the fuel equivalence ratio is small.

Acknowledgement

The authors would like to express their sincere gratitude to Dr. Satish Kumar, Mr. JVS Murthy and Mr. Rajanikanth, Scientists, Hypersonic Propulsion Division, DRDL for providing the combustor geometry, solid model of the combustor and the experimental data for the comparison purpose. We would like to thank Dr. B. S. Sarma, Technology Director, DOCD and Shri Prahlada, Director, DRDL for their continuous encouragement and keen interest in the work.

References

1. Curran, E. T., "Scramjet Engines: The First Forty Years", Jl. of Propulsion and Power, Vol. 17, No. 6, pp. 1138-1148, 2001.

2. Waltrup, P. J., "Liquid - Fueled Supersonic Combustion Ramjets: A Research Perspective", Jl. of Propulsion and Power, Vol. 3, No. 6, pp. 515-524, 1987.

3. Seiner, J. M., Dash, S. M. and Kenzakowski, D. C., "Historical Survey on Enhanced Mixing in Scramjet Engines", Jl. of Propulsion and Power, Vol. 17, No. 6, pp. 1273-1286, 2001.

4. Avrashkov, V., Baranovsky, S. and Levin, V., "Gas-Dynamic Features of Supersonic Kerosene Combustion in a Model Combustion Chamber", AIAA paper 90-5268, 1990.

5. Mathur, T., Gruber, M., Jackson, K., Donabon, J., Donaldson, W., Jackson, T. and Billig, F., "Supersonic Combustion Experiments with a Cavity-based Fuel Injector", Jl. of Propulsion and Power, Vol. 17, No. 6, pp. 1305-1312, 2001.

6. Li, J. G., Yu, G., Zhang, X. Y. and Huang, Q. S., "Combustion of Kerosene in a Supersonic Stream", AIAA paper 2000-0615, 2000.

7. Burnes, R., Parr, T. P., Wilson, K. J. and Yu, K., "Investigation of Supersonic Mixing Control Using Cavities: Effects of Fuel Injection Location", AIAA paper 2000- 3618, 2000.

8. Owens, M. G., Tehranian, S., Segal, C. and Vinogradov, V., "Flame Holding Configurations for Kerosene Combustion in a Mach 1.8 Airflow", Jl. of Propulsion and Power, Vol. 14, No. 4, pp. 456-461, 1998.

9. Vinagradov, V., Kobigsky, S. A. and Petrov, M. D., "Experimental Investigation of Kerosene Fuel Combustion in Supersonic Flow", Jl. of Propulsion and Power, Vol. 11, No. 1, pp. 130-134, 1995.

10. Ortweth, P., Mathur, A., Vinogradov, V., Grin, V., Goldfeld, M. and Starov, A., "Experimental and Numerical Investigation of Hydrogen and Ethylene Combustion in a Mach 3-5 Channel with a Single Injector", AIAA paper 96-3245, 1996.

11. Yu, K., Wilson, K. J. and Schadow, K. C., "Effects of Flame Holding on Supersonic Combustion Performance", Jl. of Propulsion and Power, Vol. 17, No.6. pp. 1287-1295, 2001.

12. Carson, R. A., Mohieldin, T. O. and Tiwari, S. N., "Numerical Study of Hydrogen and Ethylene Injected Normally in a Two Dimensional Dual-mode Scramjet Combustor", AIAA paper 2004-1035, 2004.

13. Abdel, S., Tiwari, S. N. and Mohieldin, T. O., "Study of Supersonic Combustion Characteristics in a Scramjet Combustor", AIAA paper 2003-3550, 2003.

14. Baurle, R. A. and Eklund D. R., "Analysis of Dual-mode Hydrocarbon Scramjet Operation of Mach 4-6.5", Jl. of Propulsion and Power, Vol. 18, No. 5, pp. 990- 1002, 2002.

15. White, J. A. and Morrison, J. H., "A Pseudo Temporal Multigrid Relaxation Scheme for Solving Parabolized Navier Stokes Equation", AIAA paper 1999-3360, 1999.

16. Menter, F. R., "Two Equation Eddy-viscosity Turbulence Models for Engineering Applications", AIAA Journal, Vol. 32, No. 8, pp. 1598-1605, 1994.

17. Dufour, E. and Bouchez, M. , "Computational Analysis of a Kerosene Fueled Scramjet", AIAA paper 2001-1817, 2001.

18. Bouchez, M, Dufour, E. and Montazel, X., "Hydrocarbon Fueled Scramjet for Hypersonic Vehicles", AIAA paper 1998-1589, 1998.

19. Satish Kumar, Charyulu, B. V. N, Moorthy, J. V. S. and Chandrasekhar, C., "Scramjet Combustor Development", Newsletter, The Combustion Institution (Indian Section), Vol. 25, No. 4, April 2005, pp. 16-31, 2005.

20. CFX-TASC Flow Computational Fluid Dynamics Software, Version 2.11.1, AEA Technology Engineering Software Ltd. 2001.